Cytidine diphosphate diacylglycerol synthase 2 is a synthetic lethal target in mesenchymal cancers

Tim Arnoldus
Division of Molecular Oncology and Immunology, Oncode Institute, Netherlands Cancer Institute, The Netherlands https://orcid.org/0009-0005-2104-4832

Alex van Vliet
Division of Molecular Oncology and Immunology, Oncode Institute, Netherlands Cancer Institute, The Netherlands

Adriaan de Groot
Division of Molecular Oncology and Immunology, Oncode Institute, Netherlands Cancer Institute, The Netherlands

Niek Blomberg
Center for Proteomics and Metabolomics, Leiden University Medical Center, The Netherlands

Onno Bleijerveld
Proteomics facility, Netherlands Cancer Institute, The Netherlands https://orcid.org/0000-0002-9395-2347

Susan van Hal-van Veen
Division of Molecular Oncology and Immunology, Oncode Institute, Netherlands Cancer Institute, The Netherlands

Anita Grootemaat
Electron Microscopy Centre Amsterdam, Amsterdam University Medical Center, The Netherlands

Rolf Harkes
BioImaging Facility, Netherlands Cancer Institute, The Netherlands

Nicole van der Wel
Electron Microscopy Centre Amsterdam, Amsterdam University Medical Center, The Netherlands

Maarten Altelaar
Proteomics facility, Netherlands Cancer Institute, The Netherlands; Biomolecular Mass Spectrometry and Proteomics, Utrecht University, The Netherlands https://orcid.org/0000-0001-5093-5945

Martin Giera
Center for Proteomics and Metabolomics, Leiden University Medical Center, The Netherlands https://orcid.org/0000-0003-1684-1894

Daniel Peeper (d.peeper@nki.nl)
Division of Molecular Oncology and Immunology, Oncode Institute, Netherlands Cancer Institute, The Netherlands; VU University Amsterdam, Department of Pathology, The Netherlands https://orcid.org/0000-0003-1293-3177

Article

Keywords:

Posted Date: December 7th, 2023

DOI: https://doi.org/10.21203/rs.3.rs-3626915/v1

Additional Declarations: Yes there is potential Competing Interest. T.A. and D.S.P. are named inventors on a patent application related to this work. D.S.P. is co-founder, shareholder and advisor of Immagene, which is unrelated to this study.

Abstract

Synthetic lethal interactions (SLIs) can provide a therapeutic index, as illustrated by PARP inhibition of *BRCA*-deficient cancers[1–4]. Whereas additional SLIs based on genomic alterations in cancer have been identified[5–19], we set out to explore the SLI space as a function of differential RNA expression profiles in cancer and normal tissue. By unbiased computational analyses of publicly available functional genomic and gene expression resources we uncovered a cancer-specific SLI between the paralogs cytidine diphosphate synthase 1 (*CDS1*) and *CDS2*. The essentiality of *CDS2* for cell survival is observed for mesenchymal-like cancers, which express low levels of *CDS1*. We confirm the *CDS1-2* SLI in a panel of cultured cancer cell lines and in tumor-bearing mice. Mechanistically, the *CDS1-2* SLI is accompanied by disruption of lipid homeostasis including extensive accumulation of cholesterol esters and triglycerides, and induction of apoptotic cell death. Genome-wide CRISPR-Cas9 knockout screens in a panel of *CDS1*-negative cancer cell lines failed to identify a common escape mechanism of death caused by *CDS2* ablation, indicating the robustness of the SLI. Our findings reveal that CDS2 may serve as a pharmacologically tractable target in mesenchymal cancers, meriting therapeutic exploration.

Introduction

Established SLIs in cancer

SLIs can provide a therapeutic index in cancer[1], as exemplified by the dependency on PARP of *BRCA*-deficient hereditary breast and ovarian cancer. Whereas healthy cells retain one functional germline *BRCA* copy, somatic loss of the second copy results in cancer. Because *BRCA* deficiency results in loss of homology-based DNA repair[20], it causes a strong dependency on *PARP* for genomic stability and, hence, survival. This SLI has been clinically exploited with specific PARP inhibitors[2–4]. This clinical success, and other examples, have spurred efforts to identify additional cancer-associated SLIs[5–19,21–32]. Similar to *BRCA-PARP*, data on genomic alterations specific to cancer are commonly used to find SLIs[2,3,5–20], such as the dependency on *WRN* in microsatellite unstable cancers[5,6].

Exploring SLIs in cancer based on differential gene expression

In addition to genomic alterations, cancers have also distinct gene expression profiles relative to healthy tissue. Publicly available datasets provide extensive transcriptional information as well as genetic dependencies in cancer. For example, the cancer dependency map (DepMap) is a comprehensive research initiative providing matched CRISPR screening and gene expression data for 913 cell lines across 30 cancer lineages (2021Q2)[33,34]. Additionally, the Cancer Genome Atlas (TCGA) provides genome-wide gene expression data for 9264 tumor and 741 healthy samples[35]. Together, these data sets provide approximately 1e9 datapoints on gene expression and genetic dependencies in cancer and can

be mined to predict SLIs. For example, gene expression data have been used to retrospectively predict patient responses to targeted therapy using computational synthetic lethality analyses[29].

Here, we performed unbiased computational analyses to find cancer-specific SLIs, taking advantage of these public functional genomic and gene expression resources, particularly also the Genotype-Tissue Expression project (GTEx), which provides genome-wide gene expression data for 17382 healthy tissue samples[36]. We scored all ~ 3.4e8 gene pairs for synthetic lethality and cancer specificity. We focused on the strong SLI that we uncovered between *CDS1* and *CDS2*, investigating cancer specificity, robustness of the synthetic lethal relationship *in vitro* and in mice, potential escape mechanisms, mechanism of cell death and lipidomic and proteomic analysis.

Results

Computational analyses identify CDS1-CDS2 as a common and cancer-associated SLI

To query for SLIs based on differential gene expression between cancer and normal tissue, we set up a bioinformatic pipeline using public datasets on gene dependencies and RNA expression (Fig. 1a). This pipeline identifies anchor-target gene pairs, in which the anchor gene shows a relatively reduced expression level in cancer compared to normal tissue, and in which disruption of the target gene results in cancer lethality.

The DepMap includes additional types of data that we incorporated in our pipeline to score SLIs, including promoter methylation data, protein expression data, damaging mutation data and cancer type data[33,34,37,38]. RNA expression data provided good power to detect previously established synthetic lethal interactions, including *BRCA1-PARP1* and *WRN-MLH1* (Fig. 1b, **Extended Data** Fig. 1a)[2,3,5,6,14,15,18,19,24,30,39]. The inclusion of all cancer types simultaneously resulted in a high resolution to detect established synthetic lethal interactions compared to analyzing specific cancer types separately (**Extended Data** Fig. 1a). Therefore, we determined the SLI scores for all gene pairs with RNA expression data for all cancer types simultaneously.

The *CDS1-CDS2* and *NAA10-NAA11* gene pairs received high SLI scores (Fig. 1c, **Extended Data** Fig. 1b, c **and Supplementary Table 1**). However, the *NAA10-NAA11* SLI failed to show cancer specificity and was therefore not pursued. In contrast, the *CDS1-CDS2* SLI demonstrated significant cancer specificity. The high SLI score for *CDS1-CDS2* is consistent with other analyses and screens scoring *CDS1-CDS2* as a candidate synthetic lethal pair, but to our knowledge this has not yet been pursued[18,30,32,40]. CDS1 and CDS2 are enzymes that are conserved in plants and yeast. They serve to convert phosphatidic acid into cytidine diphosphate diacylglycerol, conceivably representing the bottleneck in phosphatidylinositol (PI) synthesis[41–43]. PI constitutes an essential component of cellular membranes and is also used as a critical kinase substrate regulating cell proliferation and survival[44,45]. Aberrations in PI signaling components act as common cancer drivers and are clinically targeted with PI3K inhibitors[46].

Our analysis confirmed *FAM50A-B*, *DDX3X-DDX3Y* and *EIF1AX-EIF1AY* as cancer-specific SLIs, in agreement with previous reports (**Extended Data** Fig. 1c)[18,30]. Similarly, we identified *PARP*-associated synthetic lethality for breast cancer cell lines (Fig. 1d, **left panel**). For several other SLIs, cancer specificity was previously inferred from genomic data[5,6,14,18,19], but did not score here as such, for example *WRN-MLH1*. This is conceivably due to the relatively low frequency of genomic alterations in *MLH1* coupled to our focus on transcriptomic rather than genomic data.

In contrast, we noted that *CDS2* loss was associated with lethality in a large number of cancer types (Fig. 1d, **right panel**). Several of these concerned common cancers, including lung, blood, brain and skin cancer (**Extended Data** Fig. 1d). From here onwards, lethality as a function of *CDS2* loss will be referred to as Δ*CDS2* lethality. Patients with *CDS1*-low cancers showed significantly worse survival compared to *CDS1*-high cancer patients (Fig. 1e). For these reasons we focus here on the *CDS1-CDS2* SLI.

To confirm and quantify cancer-specific loss of *CDS1* expression, we compared pan-cancer DepMap expression data and pan-tissue GTEx expression data (Fig. 1f). The data was calibrated on housekeeping genes, while control analyses on reference genes were performed to determine reliability. In line with the TCGA data (Fig. 1c), we observed common absence, or low expression, of CDS1 in cancer cell lines compared to healthy tissue (64% average reduction, p-value < 0.0001). As expected, given the SLI, low or no CDS1 expression strongly correlated with Δ*CDS2* lethality in cancer cell lines (90% average reduction, p-value < 0.0001). We also observed that lung, blood, brain and skin cancers have reduced CDS1 levels compared to their lineages of origin (**Extended Data** Fig. 1e**)**, suggesting that these cancers may suppress transcription of *CDS1* during cancer development. For lung cancer, differential CDS1 levels were confirmed using a cohort comprising patient-matched proteomics data from healthy and tumor tissue (Fig. 1g)[47]. Thus, our *in silico* analyses predict that the *CDS1-CDS2* gene pair constitutes a human cancer-associated SLI, specifically in common *CDS1*-low cancers.

CDS1 and CDS2 constitute a synthetic lethal gene pair across cancer types

For wet lab validation of the computational predictions, we used a panel of cancer cell lines, which are also in the DepMap (Fig. 2a). Their *CDS1* RNA levels were confirmed by qPCR analysis (Fig. 2b). Low throughput CRISPR perturbations were used to quantify the lethality inferred from genome-wide CRISPR knockout screens. By including fluorescent tracker cells serving as an internal control for each experimental condition, we quantified lethality over extended timeframes, showing minimal variation (Fig. 2c).

Upon perturbation of *CDS2* with one of two separate sgRNAs, we were able to confirm Δ*CDS2* lethality in *CDS1*-low or *CDS1*-negative cell lines across several cancer types (Fig. 2d **and Extended Data** Fig. 2a, b). Furthermore, as predicted, a *CDS1*-high cell line was Δ*CDS2* non-lethal. Compared to the DepMap data, we observed remarkably strong lethality. Furthermore, Δ*CDS2* lethality was still evident in cell lines with low levels of *CDS1* RNA (Fig. 2d; green).

To validate the *CDS1* dependency for the Δ*CDS2* lethality, we either ectopically expressed *CDS1* in *CDS1*-negative cancer cell lines or perturbed *CDS1* in *CDS1*-proficient cancer cells. When *CDS1* was introduced into two *CDS1*-negative cell lines, the Δ*CDS2* lethality was largely negated. Conversely, when *CDS1* was perturbed in a *CDS1*-high cell line it exhibited increased Δ*CDS2* lethality (Fig. 2e). To validate these observations, we admixed control GFP-expressing cancer cell lines with *CDS1*-restored cell lines in an additional panel of four human melanoma models. The results confirmed strong synthetic lethality upon perturbation of *CDS2* in this panel (Fig. 2f **and Extended Data** Fig. 2c). Together, these functional experiments confirm that *CDS1* and *CDS2* constitute a synthetic lethal pair across a panel of cancer cell lines *in vitro*.

ΔCDS2 lethality is associated with apoptosis

We suspected Δ*CDS2* lethality may result in apoptotic cell death *in vitro*. To investigate this, we collected tumor samples and measured cleaved caspase-3 by quantitative western blotting as a measure of apoptosis (Fig. 2g). For quantification the cleaved caspase-3 signal is compared to total protein signal in the same capillary. As a positive control, we analyzed cleaved caspase-3 levels upon induction of apoptosis by TPCA-1 + TNF (BLM) or staurosporine (SK-MEL-2) (**Extended Data** Fig. 2d). We observed a significant increase in cleaved caspase-3 in Δ*CDS2* cancer cells, which indicates Δ*CDS2* lethality is associated with tumor cell apoptosis.

ΔCDS2 lethality in vivo

Next, we investigated whether the SLI between *CDS1* and *CDS2* observed *in silico* and *in vitro* can be recapitulated *in vivo*. For this purpose, we again admixed control GFP-expressing cancer cell lines with *CDS1*-restored cell lines. Tumor cells were inoculated into immunodeficient NOD-Scid IL2Rgnull mice and analyzed by flow cytometry of the tumors 17 days later. We observed a striking inability of *CDS2*-perturbed cells to contribute to tumor formation *in vivo* (Fig. 2h **and Extended Data** Fig. 2e, f; note that the tumor growth curves are derived from cell mixes including rescued cells). Together, these results demonstrate that *CDS1* and *CDS2* form a robust synthetic lethal pair in cancer, *in silico*, *in vitro* and *in vivo*.

No common escape mechanism for Δ CDS2 lethality

The computational and *in vitro* and *in vivo* functional validation data above demonstrate the broad cancer range and reproducibility of the *CDS1-2* SLI, prompting us to further challenge its robustness. Specifically, the rate-limiting role of the CDS enzymes in PI synthesis led us to investigate whether any cells can rewire their signaling network such that they can escape from this SLI. To investigate this in an unbiased, genome-wide fashion, we performed CRISPR knockout rescue screens in a panel of four *CDS1*-negative human cancer cell lines and, as a control, one *CDS1*-high cancer cell line (Fig. 3a **and Supplementary Table 2**). In parallel, cells from the screens were used to track Δ*CDS2* lethality during the screen. These analyses confirmed Δ*CDS2* lethality in four *CDS1*-negative cancer cell lines and extended our data on the lack of Δ*CDS2* lethality in *CDS1*-high cancer cell lines to an additional cancer cell line

(Fig. 3b). In addition, colony formation assays were performed to visualize the lethal effect during the screen (**Extended Data** Fig. 3a; note that for K562 a different readout was used because it is a suspension cell line).

Analysis of the dropout of essential genes confirmed the high quality of the screens (Fig. 3c). Potential escape mechanisms were determined using Δ*CDS2* lethality quantified with tracker cells. However, the results of the screens (Fig. 3d **and Extended Data** Fig. 3b) indicated no common escape mechanism of Δ*CDS2* lethality. For example, the screen performed in SK-MEL-2 cells yielded no significant enrichment even after an additional 14 days (32 days in total; **Extended Data** Fig. 3c), while the other screens yielded only some cell line-specific rescue (**Extended Data** Fig. 3d-f). These findings suggest that no common escape to the combined loss of *CDS1* and *CDS2* is possible, which is in agreement with the idea that CDS1 and CDS2 together serve as a bottleneck for PI synthesis.

Mesenchymal cancers depend on CDS2 for PI synthesis

To understand which cancer types show reduced *CDS1* expression and, hence, Δ*CDS2* lethality, we characterized *CDS1*-low cancers using publicly available data. First, we noted that *CDS1*-high cancer cells express high levels of the epithelial marker gene E-cadherin, whereas *CDS1*-low cancer cell lines instead express mesenchymal markers like ZEB1, ZEB2 and vimentin (Fig. 4a **and Extended Data** Fig. 4a)[48,49]. Mechanistically, this is in agreement with the notion that *CDS1* expression is suppressed in mesenchymal cancers by the transcription factor ZEB1, previously reported to bind the *CDS1* locus and to suppress *CDS1* expression[50,51]. Besides this major regulatory mechanism, we also observed that a rare subset of the blood lineage cancer cell lines exhibit methylation of the *CDS1* promoter (**Extended Data** Fig. 4b). Overall, these findings indicate that the suppression of *CDS1* expression in mesenchymal-like cancers (by ZEB1) results in their strong dependency on *CDS2*.

Gene-set enrichment analysis indicated that *CDS1*-low cancers are enriched for the Hallmark EMT gene-set ($p = 0.0001$ DepMap, $p = 0.009$ TCGA, **Extended Data** Fig. 4c). Mesenchymal-transitioned cancers are common, highly metastatic and therapy-refractory[48,52–55]. These findings are in agreement with our observations that low *CDS1* expression is common, more frequent in cancers compared to their healthy tissue of origin and associated with worse survival (Fig. 1d, e, **Extended Data** Fig. 1e). Together, these results suggest that suppression of *CDS1* expression is an integral element of EMT in cancer.

Next, we zoomed in into the pathway in which CDS1 and CDS2 are involved, as has been defined by previous studies (Fig. 4b)[41–43,56]. We incorporated expression and dependency data from the DepMap of the enzymes involved. In line with the requirement for CDS1/2, the next enzyme in the pathway, cytidine diphosphate diacylglycerol synthase inositol-3-phosphatidyltransferase (CDIPT), is highly essential for survival. In addition, *CDS2* and *CDIPT* are significantly co-dependent in DepMap cancer cell lines, which is indicative of a similar mechanism of dependency (Fig. 4c)[27,57]. Accordingly, when supplementing the cell culture media with exogenous PI, we observed a significant rescue of cell death, suggesting that Δ*CDS2* lethality is due, at least in part, to insufficient availability of PI (Fig. 4d **and Extended Data** Fig. 4d).

CDS2 acts upstream of the PI3K signaling module regulating growth and survival. Unexpectedly, DepMap analysis revealed that Δ*CDS2* lethality is not accompanied by lethality with either genetic loss of *PIK3CA* or pharmacologic PIK3CA inhibition (Alpelisib). Instead, we observed a strong anticorrelation between Δ*CDS2* lethality and Δ*PI3KCA* lethality (Fig. 4c). This anticorrelation was independent of PI3K isoforms, as judged by pan-PI3K inhibitor responses. These results demonstrate an essential role of *CDS* for PI synthesis in mesenchymal cancers. Furthermore, they unexpectedly point to a contribution of *CDS1* and *CDS2* to survival signaling independent of the classical PI3K pathway.

Expression of either CDS1 or CDS2 is required for lipid homeostasis

To biochemically define the effects of *CDS2* perturbation in *CDS1*-negative cancer cells, we performed multi-omic analyses in a panel of four *CDS1*-negative cancer cell lines and, as a control, one *CDS1*-high cancer cell line (Fig. 5a). Lipidomics was performed to quantify buildup or depletion of lipids, specifically those in the CDS pathway. In addition, proteomics was performed to identify deregulated cellular processes upon CDS2 loss.

Lipidomic analysis allowed for quantification of the major lipid classes in the cells, with phosphorylated PI (PIP) serving as the major signaling molecule[44] (**Extended Data** Fig. 5a **and Supplementary Table 3**). Major changes as a function of *CDS1* expression were detected upon CDS2 loss (Fig. 5b **and Extended Data** Fig. 5a, b; note that the stars indicate the number of *CDS1*-negative cancer cell lines with p-value < 0.01). For example, cholesterol esters and triglycerides were massively upregulated. Furthermore, we observed strong buildup of CDS2 substrates and depletion of the downstream product PI.

The proteomics analysis allowed for quantification of ~ 7000 proteins in each cell line (**Supplementary Table 4**). As expected, the levels of CDS2 protein had dropped 10-fold in all five cell lines upon *CDS2* CRISPR perturbation (Fig. 5c). In addition, large groups of proteins were commonly and significantly down- or up-regulated in *CDS1*-low cancer cell lines, suggesting an orchestrated response (Fig. 5c **and Extended Data** Fig. 5c). GO-term enrichment analysis of these proteins revealed major induction of cholesterol import and production upon Δ*CDS2* lethality (**Extended Data** Fig. 5d).

In line with the build-up of cholesterol esters and triglycerides, *CDS2*-perturbed cells formed large lipid droplets[58], which were visible by both light and electron microscopy, staining positively for the lipid dyes BODIPY and Nile Red. Quantification of BODIPY-stained live cells revealed that on average 3% of the imaged cells comprised lipid (Fig. 5d). Combined light and electron microscopy of fixed cells showed these lipid droplets in more detail (Fig. 5e). Together, these findings again corroborate the CDS1/2 biochemical bottleneck to support lipid homeostasis, demonstrating that lethality upon *CDS2* perturbation in *CDS1*-low cell lines is accompanied by major changes in lipid metabolism and expression of the cholesterol pathway (Fig. 5f).

Discussion

Genomic alterations in cancer can serve as a mechanistic basis for SLIs[2,3,5–19]. Cancers show also distinct gene expression patterns compared to healthy tissue, prompting us to explore the cancer SLI space based on differential gene expression in normal and healthy tissue. Taking advantage of extensive publicly available cancer datasets, we identify here by computational mining that CDS2 serves as a synthetic lethal target in mesenchymal cancers. Our bioinformatic pipeline revealed a potential therapeutic index thanks to differential *CDS1* expression in cancer cells (low) and normal cells (high). We confirmed that *CDS1* and *CDS2* constitute a functional SLI across many cancer types, particularly those of mesenchymal origin, representing approximately 40% of all cancers. The SLI is mechanistically explained by the fact that the combined loss of *CDS1* and *CDS2* is incompatible with cell survival, in combination with the low or absent expression of *CDS1* in mesenchymal cancer cells resulting in Δ*CDS2* lethality. Our data are in agreement with results by Chan et al. reporting that *CDS1-2* are a synthetic lethal gene pair in uveal melanoma (co-submitted to *Nature Genetics* with this manuscript).

A series of CRISPR knockout rescue screens confirmed not only the synthetic lethal relationship between *CDS1* and *CDS2*, but also that they form a bottleneck in a pathway required for PI synthesis that apparently is essential for cancer cell viability. Mechanistically, we show that Δ*CDS2* lethality causes cancer cell apoptosis, which can be rescued at least in part by supplementing exogenous PI. The latter is consistent with a requirement for CDS2 to produce PI. Our data also strongly suggest that, unexpectedly, PI synthesis is required for cell survival independent of classical PI3K-dependent survival signaling, because cell lines that depend on *CDS1/2* for survival did not require PI3K. Our data imply that CDS2 inhibition may be explored to eliminate particularly mesenchymal-like cancers, which are common, highly metastatic and therapy-refractory[48,52–55].

To date, no inhibitor is available for CDS2 targeting. However, assuming that its enzymatic activity is involved, pharmacological targeting may be possible. For example, for PI3K and DGAT enzymes acting in the same pathway inhibitors exist, while for PI3K inhibition isoform-specific inhibitors also are available[46]. Because healthy tissues are not included in the DepMap data, we cannot exclude that dose-limiting toxicities for CDS2 inhibition may occur. Reassuringly however, the GTEx data suggests that high expression of *CDS1* is ubiquitous across healthy tissues. Furthermore, CDS2-targeting morpholinos are tolerated in mice[59]. We would propose to develop a CDS2-specific inhibitor to maximize the therapeutic index; this may be possible given the different acyl-chain preferences for CDS2 and CDS1[43]. Clearly, a CDS2-specific inhibitor would be required to determine whether, as our large-scale computational and functional data *in vitro* and *in vivo* predict, a therapeutic index for clinically exploiting the *CDS1-2* SLI exists.

Declarations

Acknowledgements

We acknowledge David Adams and Pui Ying Chan for sharing unpublished data and coordinating submission of the manuscripts. We acknowledge Eva Hernando for sharing a SK-MEL-147 STR reference

profile. We are grateful to Thijs Jalving and Sebastiaan Schieven for checking some data processing. We acknowledge support for proteomics by the X-omics Initiative (Project 184.034.019), part of the NWO National Roadmap for Large-Scale Research Infrastructures. D.S.P. is funded by the Oncode Institute, which is partly financed by the Dutch Cancer Society KWF. Research at the Netherlands Cancer Institute is supported by institutional grants of the Dutch Cancer Society and the Dutch Ministry of Health, Welfare and Sport.

Author contributions

T.A. designed the study, performed analyses, performed experiments, and wrote the manuscript; A.v.V. performed analyses; A.d.G. performed experiments; N.B. and M.G. measured lipidome levels; O.B. and M.A. measured proteome levels; S.v.H. measured mouse tumors; R.H. performed BODIPY analysis; A.G. and N.v.d.W. performed electron microscopy; D.S.P. designed the study, supervised the study, wrote the manuscript and provided funding.

Competing interest declaration

T.A. and D.S.P. are named inventors on a patent application related to this work. D.S.P. is co-founder, shareholder and advisor of Immagene, which is unrelated to this study.

References

1. Hartwell, L. H., Szankasi, P., Roberts, C. J., Murray, A. W. & Friend, S. H. Integrating genetic approaches into the discovery of anticancer drugs. *Science* **278**, 1064–1068 (1997).
2. Bryant, H. E. *et al.* Specific killing of BRCA2-deficient tumours with inhibitors of poly(ADP-ribose) polymerase. *Nature* **434**, 913–917 (2005).
3. Farmer, H. *et al.* Targeting the DNA repair defect in BRCA mutant cells as a therapeutic strategy. *Nature* **434**, 917–921 (2005).
4. Fong, P. C. *et al.* Inhibition of Poly(ADP-Ribose) Polymerase in Tumors from *BRCA* Mutation Carriers. *N. Engl. J. Med.* **361**, 123–134 (2009).
5. Chan, E. M. *et al.* WRN helicase is a synthetic lethal target in microsatellite unstable cancers. *Nature* **568**, 551–556 (2019).
6. Kategaya, L., Perumal, S. K., Hager, J. H. & Belmont, L. D. Werner Syndrome Helicase Is Required for the Survival of Cancer Cells with Microsatellite Instability. *iScience* **13**, 488–497 (2019).
7. Muller, F. L. *et al.* Passenger deletions generate therapeutic vulnerabilities in cancer. *Nature* **488**, 337–342 (2012).
8. Mavrakis, K. J. *et al.* Disordered methionine metabolism in MTAP/CDKN2A-deleted cancers leads to dependence on PRMT5. *Science* **351**, 1208–1213 (2016).
9. Kryukov, G. V. *et al.* MTAP deletion confers enhanced dependency on the PRMT5 arginine methyltransferase in cancer cells. *Science* **351**, 1214–1218 (2016).

10. Zhao, D. *et al.* Synthetic essentiality of chromatin remodelling factor CHD1 in PTEN-deficient cancer. *Nature* **542**, 484–488 (2017).
11. Lee, R. *et al.* Synthetic Essentiality of Tryptophan 2,3-Dioxygenase 2 in APC-Mutated Colorectal Cancer. *Cancer Discov.* **12**, 1702–1717 (2022).
12. Jerby-Arnon, L. *et al.* Predicting cancer-specific vulnerability via data-driven detection of synthetic lethality. *Cell* **158**, 1199–1209 (2014).
13. Frezza, C. *et al.* Haem oxygenase is synthetically lethal with the tumour suppressor fumarate hydratase. *Nature* **477**, 225–228 (2011).
14. Oike, T. *et al.* A synthetic lethality-based strategy to treat cancers harboring a genetic deficiency in the chromatin remodeling factor BRG1. *Cancer Res.* **73**, 5508–5518 (2013).
15. Hoffman, G. R. *et al.* Functional epigenetics approach identifies BRM/SMARCA2 as a critical synthetic lethal target in BRG1-deficient cancers. *Proc. Natl. Acad. Sci. U. S. A.* **111**, 3128–3133 (2014).
16. Helming, K. C. *et al.* ARID1B is a specific vulnerability in ARID1A-mutant cancers. *Nat. Med.* **20**, 251–254 (2014).
17. Feng, X. *et al.* Genome-wide CRISPR screens using isogenic cells reveal vulnerabilities conferred by loss of tumor suppressors. *Sci. Adv.* **8**, 6638 (2022).
18. Köferle, A. *et al.* Interrogation of cancer gene dependencies reveals paralog interactions of autosome and sex chromosome-encoded genes. *Cell Rep.* **39**, 110636 (2022).
19. Neggers, J. E. *et al.* Synthetic Lethal Interaction between the ESCRT Paralog Enzymes VPS4A and VPS4B in Cancers Harboring Loss of Chromosome 18q or 16q. *Cell Rep.* **33**, 108493 (2020).
20. Venkitaraman, A. R. Cancer susceptibility and the functions of BRCA1 and BRCA2. *Cell* **108**, 171–182 (2002).
21. Tong, A. H. Y. *et al.* Systematic genetic analysis with ordered arrays of yeast deletion mutants. *Science* **294**, 2364–2368 (2001).
22. Pan, X. *et al.* A robust toolkit for functional profiling of the yeast genome. *Mol. Cell* **16**, 487–496 (2004).
23. Costanzo, M. *et al.* The genetic landscape of a cell. *Science* **327**, 425–431 (2010).
24. van Delft, M. F. *et al.* The BH3 mimetic ABT-737 targets selective Bcl-2 proteins and efficiently induces apoptosis via Bak/Bax if Mcl-1 is neutralized. *Cancer Cell* **10**, 389–399 (2006).
25. Shalem, O. *et al.* Genome-scale CRISPR-Cas9 knockout screening in human cells. *Science* **343**, 84–87 (2014).
26. Wang, T., Wei, J. J., Sabatini, D. M. & Lander, E. S. Genetic screens in human cells using the CRISPR-Cas9 system. *Science* **343**, 80–84 (2014).
27. Tsherniak, A. *et al.* Defining a Cancer Dependency Map. *Cell* **170**, 564-576.e16 (2017).
28. Lee, J. S. *et al.* Harnessing synthetic lethality to predict the response to cancer treatment. *Nat. Commun.* **9**, 1–12 (2018).

29. Lee, J. S. *et al.* Synthetic lethality-mediated precision oncology via the tumor transcriptome. *Cell* **184**, 2487-2502.e13 (2021).
30. Thompson, N. A. *et al.* Combinatorial CRISPR screen identifies fitness effects of gene paralogues. *Nat. Commun.* **12**, 1302 (2021).
31. Dede, M., McLaughlin, M., Kim, E. & Hart, T. Multiplex enCas12a screens detect functional buffering among paralogs otherwise masked in monogenic Cas9 knockout screens. *Genome Biol.* **21**, 1–19 (2020).
32. Parrish, P. C. R. *et al.* Discovery of synthetic lethal and tumor suppressor paralog pairs in the human genome. *Cell Rep.* **36**, 109597 (2021).
33. DepMap 21Q2 Public. Available at: https://figshare.com/articles/dataset/DepMap_21Q2_Public/14541774/2. (Accessed: 20th October 2021)
34. Meyers, R. M. *et al.* Computational correction of copy number effect improves specificity of CRISPR-Cas9 essentiality screens in cancer cells. *Nat. Genet.* **49**, 1779–1784 (2017).
35. Weinstein, J. N. *et al.* The cancer genome atlas pan-cancer analysis project. *Nat. Genet.* **45**, 1113–1120 (2013).
36. Lonsdale, J. *et al.* The Genotype-Tissue Expression (GTEx) project. *Nature Genetics* **45**, 580–585 (2013).
37. Nusinow, D. P. *et al.* Quantitative Proteomics of the Cancer Cell Line Encyclopedia. *Cell* **180**, 387-402.e16 (2020).
38. Ghandi, M. *et al.* Next-generation characterization of the Cancer Cell Line Encyclopedia. *Nature* **569**, 503–508 (2019).
39. DeWeirdt, P. C. *et al.* Genetic screens in isogenic mammalian cell lines without single cell cloning. *Nat. Commun.* **11**, 1–15 (2020).
40. Lin, H. K. *et al.* Functional buffering via cell-specific gene expression promotes tissue homeostasis and cancer robustness. *Sci. Rep.* **12**, 2974 (2022).
41. Halford, S., Dulai, K. S., Daw, S. C., Fitzgibbon, J. & Hunt, D. M. Isolation and chromosomal localization of two human CDP-diacylglycerol synthase (CDS) genes. *Genomics* **54**, 140–144 (1998).
42. Volta, M. *et al.* Identification and characterization of CDS2, a mammalian homolog of the Drosophila CDP-diacylglycerol synthase gene. *Genomics* **55**, 68–77 (1999).
43. D'Souza, K., Kim, Y. J., Balla, T. & Epand, R. M. Distinct properties of the two isoforms of CDP-diacylglycerol synthase. *Biochemistry* **53**, 7358–7367 (2014).
44. Goncalves, M. D., Hopkins, B. D. & Cantley, L. C. Phosphatidylinositol 3-Kinase, Growth Disorders, and Cancer. *N. Engl. J. Med.* **379**, 2052–2062 (2018).
45. Cantley, L. C. The phosphoinositide 3-kinase pathway. *Science* **296**, 1655–1657 (2002).
46. Vanhaesebroeck, B., Perry, M. W. D., Brown, J. R., André, F. & Okkenhaug, K. PI3K inhibitors are finally coming of age. *Nature Reviews Drug Discovery* **20**, 741–769 (2021).

47. Satpathy, S. *et al.* A proteogenomic portrait of lung squamous cell carcinoma. *Cell* **184**, 4348-4371.e40 (2021).
48. Yang, J. & Weinberg, R. A. Epithelial-Mesenchymal Transition: At the Crossroads of Development and Tumor Metastasis. *Developmental Cell* **14**, 818–829 (2008).
49. Mak, M. P. *et al.* A Patient-Derived, Pan-Cancer EMT Signature Identifies Global Molecular Alterations and Immune Target Enrichment Following Epithelial-to-Mesenchymal Transition. *Clin. Cancer Res.* **22**, 609–620 (2016).
50. Gemmill, R. M. *et al.* ZEB1-responsive genes in non-small cell lung cancer. *Cancer Lett.* **300**, 66–78 (2011).
51. Feingold, E. A. *et al.* The ENCODE (ENCyclopedia of DNA Elements) Project. *Science* **306**, 636–640 (2004).
52. Mani, S. A. *et al.* The Epithelial-Mesenchymal Transition Generates Cells with Properties of Stem Cells. *Cell* **133**, 704–715 (2008).
53. Hanahan, D. & Weinberg, R. A. Hallmarks of cancer: the next generation. *Cell* **144**, 646–74 (2011).
54. Fischer, K. R. *et al.* Epithelial-to-mesenchymal transition is not required for lung metastasis but contributes to chemoresistance. *Nature* **527**, 472–476 (2015).
55. Van Espen, B. *et al.* RNF185 Control of COL3A1 Expression Limits Prostate Cancer Migration and Metastatic Potential. *Mol. Cancer Res.* OF1–OF14 (2023). doi:10.1158/1541-7786.MCR-23-0512
56. Bateman, A. *et al.* UniProt: the Universal Protein Knowledgebase in 2023. *Nucleic Acids Res.* **51**, D523–D531 (2023).
57. Wainberg, M. *et al.* A genome-wide atlas of co-essential modules assigns function to uncharacterized genes. *Nat. Genet.* **53**, 638–649 (2021).
58. Olzmann, J. A. & Carvalho, P. Dynamics and functions of lipid droplets. *Nature Reviews Molecular Cell Biology* **20**, 137–155 (2019).
59. Stratman, A. N. *et al.* Anti-angiogenic effects of VEGF stimulation on endothelium deficient in phosphoinositide recycling. *Nat. Commun.* **11**, 1–14 (2020).

Methods

Software

Flow cytometry data was analyzed using Flowjo (v10.6.0). For data analysis and statistics Excel (16.71), R (4.2.2), Rstudio (2023.03.0 + 386) or Graphpad Prism (9.4.1) was used. Quantitative elements of figures were generated using Graphpad Prism or Flowjo. Visual elements of graphs and plots were designed and generated in Adobe Illustrator (26.2). MAGeCK v0.5.9.5 was used for screen analysis[60]. Image analysis by macro was performed using FIJI 2.14.0, Java 1.8.0 and ImageJ 1.54f[61].

Data processing & availability

Data processing was always verified by a second researcher. Complex bioinformatic analyses were redone independently. For these analyses, software notebooks designed to ease reproduction are available on Figshare. Files required to run the provided software are either directly supplied or instructions for downloading are supplied. Unprocessed proteomic data are available on the Proteomics IDEntifications repository (PXD045833). All other plotted and unprocessed data related to this study are available on Figshare.

Review repository access information

Figshare reviewer acces

https://figshare.com/s/5a4ee85512d58ab924aa

PRIDE reviewer access

Username reviewer_pxd045833@ebi.ac.uk

Password kvmhgerD

Cancer-specific synthetic lethality prediction

Briefly, to rank potential synthetic lethal candidate pairs, the Pearson correlation between fitness data (CERES) and mRNA expression, proteomics, mutation or methylation data was calculated with 21Q2 DepMap data. Each pair includes the anchor gene (expression gene) and the target gene (fitness effect gene), respectively. To validate this approach, several positive control synthetic lethal pairs were selected. Positive control analyses were run using all pairs with the anchor genes. To identify the most promising new synthetic lethal interactions, the anchored approach was replaced with a genome-wide analysis encompassing 3.4e8 gene pairs. From the results, the top pair for each anchor was ranked to form a hit list. Then, all duplicate target genes were removed to prevent false positives from cross-correlated anchor genes. Reanalyzed TCGA RNA data and healthy or tumor annotation was downloaded from accession GSE62944[62]. The fold change in expression was calculated for each anchor gene in the synthetic lethality prediction.

Patient mortality and survival analysis

TCGA pan cancer atlas RNA and outcome data was downloaded on Januari 12th 2023 from:

https://gdc.cancer.gov/about-data/publications/pancanatlas

United States patient mortality data by cancer type was collected on Januari 18th 2023 from:

https://seer.cancer.gov/archive/csr/1975_2017/results_single/sect_01_table.04_2pgs.pdf

21Q2 DepMap data for cell lines with available RNA and dependency data was used for Δ*CDS2* lethality. Lineages of patient mortality data and DepMap data were matched manually (**Supplementary Table 5**).

Comparing CDS1 expression between healthy tissue and cancer cell lines

GTEx v8 TPM was downloaded from the portal on January 1st 2022. 21Q2 DepMap data was downloaded from the DepMap portal. Calibration genes with available TPM in DepMap and GTEx were used for normalization[63]. Up- and down- regulation controls were selected from literature[64,65]. Briefly, transcripts per million for each calibration gene were normalized to their own average expression. Then the TPM for *B2M, CDS1, CDKN2B* and *E2F1* were normalized to the average of the calibration gene expression. Calibrated results are similar to uncalibrated results due to intrinsic total RNA calibration of the GTEx and DepMap dataset TPM data. The analysis was also performed for blood, skin, lung and brain lineage data with the original labelling from the DepMap and GTEx, also including soft tissue ATRT in the DepMap brain category.

Healthy and tumor proteome data

Tumor and normal adjacent lung proteome data from Satpathy et al. was downloaded from entry PDC000234 and analyzed[47]. Specifically, log2-transformed ratios to internal controls were collected and sample names were mapped to their healthy or tumor tissue origin. Before plotting and statistical testing log2-transformation was undone resulting in ratios to internal control. The internal control was reported to be a mix of all samples. Still, calibration genes with available ratios in all samples were used for normalization[63]. Each calibration gene ratio was normalized to its own average ratio. Then the ratio for CDS1 was normalized to the geometric mean of the normalized calibration gene ratios for each sample.

Quantitative polymerase chain reaction to quantify RNA

Three housekeeping genes for calibration were selected from a previously described list of options based on stable pan-cancer cell line expression in the DepMap[63]. qPCR was performed as previously described[66]. The average of quadruplicate CT values was calculated for each gene. To normalize to calibration genes the geometric mean of the three calibration gene CT values was subtracted from the CDS1 CT value. To normalize to A431, the CT value of A431 was subtracted from the other cell line CT values. By exp2 CT values were transformed to fold changes.

Forward primer (5’ to 3’) Reverse primer (5’ to 3’)
CHMP2A CGCGAGCGACAGAAACTAGAG CCCGCATCAATACAAACTTGC

VPS29 TGCAACAGTTTGCCAGCTAAA CCTCTGCAACAGGGCTAAGC

PSMB2 ATCCTCGACCGATACTACACAC GAACACTGAAGGTTGGCAGAT

CDS1 CCTTGTCATCCAAAATCTGT GAATCCTTCCCAAGTCTTTT

Lentiviral transduction

Cell lines were lentivirally transduced as previously described[66]. Transduced cells were always kept on selection during cell culture *in vitro.* The complete selection was verified by the loss of the control

untransduced cells on selection. Low throughput CRISPR perturbation using pLentiCRISPR v2 Puro or Blast and ectopic expression using pLX304 Blast (*CDS1* & GFP)[67] or pCDH Puro (mCherry) was performed as previously described[66,68]. For Fig. 2e Blast resistance was introduced to mCherry-transduced cells using pLentiCRISPR v2 Blast. In Fig. 2d sg*CDS2* #1 and #2 were used and for all other experiments sg*CDS2* #2 was used. In Fig. 2e sg*CDS1* was introduced using pLentiCRISPR v2 Blast.

sg*CDS1*:
5' GTGTCGCCGCCACACCGCGA 3'

sg*CDS2* #1:
5' ACCAGGGCAGATCATATGAG 3'

sg*CDS2* #2:
5' AGTAAAGGAAATGAACCGG 3'

sgControl:
5' AGCTTTCGAAATTGAGTGTC 3'

Determining (synthetic) lethality by tracking fluorescent cells

Briefly, after lentiviral transduction (1 day) and puromycin selection of sgRNA-transduced cells (2 days) the indicated cell mixes were prepared. For the *in vivo* experiments cells were selected one day longer. To determine lethality sgRNA-transduced cells were mixed with non-sgRNA transduced mCherry-positive cells. On the day of mixing (day 0) and at the indicated later time points samples from each cell mix were analyzed by flow cytometry to determine the ratio between negative and positive cells. Final ratios were normalized to day 0 ratios and to sgControl ratios. For lethality, normalized ratios were transformed into percentages to get survival percentages and subtracted from 100 to get lethality percentages. To determine synthetic lethality ectopic *CDS1*- or GFP-expressing cells, both transduced with the same sgRNA, were mixed on day 0. Then, lethality was calculated for the GFP-positive cells in an identical manner as for the mCherry-negative cells.

Flow cytometry

Flow cytometry data was collected on a BD Fortessa flow cytometer regularly maintained in the NKI flow cytometry facility. One of several live/dead dyes was always included: DAPI (D9542-50MG, Sigma), PI (537059-100MG, Merck), DRAQ7 (D15106, Thermofisher) and fixable near IR (L34976, Thermofisher). 0.1% BSA in PBS was used as a washing and staining solution. Samples were washed three times (including resuspension as one wash) in 0.1% BSA in PBS, once for dead cell experiments to preserve dead cells and six times for *in vivo* samples to reduce post-digestion debris. The gating strategies used are presented in **Extended Data Fig. 6**.

Cell line culture

Cell lines were cultured in DMEM (41966052, Gibco) 10% FCS (3101120, Sigma) or RPMI (21875034, Thermofisher) 10% FCS for lung and blood cancer cell lines. Cells were passaged at subculturing ratios corresponding to 80% confluence at the next passage. During experiments medium was supplemented with penicillin & streptomycin (P/S, 15140122, Invitrogen).

Cell lines were authenticated using the STR profiling kit from Promega (B9510). BLM was profiled by Eurofins (**Supplementary Table 6**). Public references were available for all cell lines except SK-MEL-147 and BLM. For SK-MEL-147 a reference the was requested via private correspondence[69]. Cells in culture were screened for mycoplasma monthly[70].

Immunoblotting

Quantitative westerns (Abby) for cleaved caspase-3 (primary 9664S; CST) with total protein were prepared and ran according to the manufacturer's instructions with the manufacturer's reagents. CRISPR-perturbed samples for cell death analysis were split on day 11 after transduction and harvested on day 12 after transduction. Samples for immunoblotting by simple western were collected as previously described with the additional inclusion of the floating cell fraction[66]. As a control, we measured cleaved caspase-3 upon induction of apoptosis with 1 µM staurosporine (9953S, CST) in SK-MEL-2 or 200 ng/mL TNF (11343017, Immunotools) + 10 µM TPCA-1 (S2824, Selleckchem) in BLM[71,72].

Animal studies

All animal studies were approved by the animal ethics committee of the Netherlands Cancer Institute (NKI) and performed under approved NKI CCD (Centrale Commissie Dierproeven) projects according to the ethical and procedural guidelines established by the NKI and Dutch legislation. Mice were housed in single-use standard cages at controlled filtered air humidity (55%), temperature (21°C) and light cycle. All housing material, food and water were autoclaved or irradiated before use. Animal husbandry was previously described[66]. Synthetic lethality *in vivo* was quantified as it was *in vitro* with the following adaptations. Puromycin selection was not continued *in vivo*. 2e6 melanoma cell mixes prepared on day 0 were injected subcutaneously into the flank of weight-randomized 13–15 week-old NOD-Scid IL2Rgnull mice (Jax). Mice were numbered and researchers were blinded from this step onwards. Tumor sizes were measured by caliper. Tumors were harvested, digested and processed into homogeneous single cell solutions. Then samples were stained for human B2M (316320, Biolegend) to exclude mouse cells and analyzed by flow cytometry. Results were normalized to day 0 and sgControl. For each group one sample was unblinded during flow cytometry acquisition to set voltages and gates for all groups.

Genome-wide CRISPR perturbation

Screening was performed as published previously[68,73,74]. The one vector Brunello library was amplified in liquid culture at 20.000x coverage and maintenance of the original sgRNA distribution was confirmed.

Screen cells were transduced at an MOI of 0.3–0.7 with Polybrene (TR-1003-G, Sigma) at 8 µg/mL. Screens were performed at 200x coverage. Novaseq was used to sequence the screen samples and the amplified Brunello library. The following sequencing primers with unique dual indexes per sample were used:

Forward sequencing primer (N = unique index for each sample)
5’ AATGATACGGCGACCACCGAGATCTACACNNNNNNNNACACTCTTTCCCTACACGAC

GCTCTTCCGATCTTCTTGTGGAAAGGACGAAACACCG 3’

Reverse sequencing primer (N = unique index for each sample)
5’ CAAGCAGAAGACGGCATACGAGATNNNNNNNNGTGACTGGAGTTCAGACGTGTGCT

CTTCCGATCTCGACTCGGTGCCACTTTTTCAAGTT 3’

To allow drop-out of essential sgRNAs, cells were cultured for 10 days after Brunello library transduction. After single sgControl and sg*CDS2* lentivirus transduction cells were cultured for 18 days. For SK-MEL-2 comparatively little cells were available due to lethality and no hits were detected. To ensure detection of any escape mechanism, a cryopreserved sample from day 7 was cultured until day 32 after single sgControl and sg*CDS2* transduction, and those results were used for the presented analyses.

The colony formation assays were started with screen cells on day 8. For K562, MCF7, NCI-H2030, LPS141 and SK-MEL-2 cell lines, 125.000, 125.000, 62.500, 31.250 and 125.000 cells were seeded, respectively. The crystal violet stainings were done when control cells had reached confluence, which was after 4, 14, 12, 7 and 12 days, respectively. A seeding density corresponding to the longest culture time for MCF7 was chosen to ensure maximum sensitivity for detecting a potential difference. For K562 suspension cells, the cells were instead counted with Trypan Blue using an automatic cell counter (Biorad TC20). In addition, lethality was tracked from day 8 until day 19 using tracker cells and used to calculate rescue percentages. The quality control ROC-AUC curves were generated as described previously[73].

Lethality and synthetic lethality rescue experiments

For the synthetic lethality rescue experiments the method to track synthetic lethality by tracking GFP-positivity was used. The indicated cell mixes were generated 10 days after transduction with sgControl or sg*CDS2* lentivirus. After overnight attachment, treatment was started and samples were harvested to measure GFP positivity at starting point. Cells were split and refreshed on day 3 and measured on day 7 after start of treatment. Phospholipids were complexed with BSA. 500 µM stock solutions were generated by incubating phospholipid with 2.5% fatty-acid free BSA from Sigma (#A8806) in DMEM at 37°C for 1 hour. Liver PC (840055P-25MG) or PI (840042P-25MG) from Avanti Polar Lipids was used. Final GFP-/GFP + ratios were normalized to input ratios and sgControl ratios to obtain the synthetic lethal fraction. For rescue, the fold change in the synthetic lethal fraction was calculated by dividing by the untreated synthetic lethal fractions and transformed into rescue percentages by subtraction from 1 and multiplication by 100. The resulting rescue percentages correspond to the part of the total synthetic

lethality that was negated in the treated conditions. For the overnight lethality rescue, CRISPR-perturbed samples for cell death analysis were split on day 11 after transduction and harvested on day 12 after transduction. PI (840042P-100MG) from Avanti Polar Lipids was dissolved in medium and added to the cells at 2 mM.

Gene set enrichment analyses

Hallmark gene set enrichment analyses were performed using GSEA 4.1.0 (Java tool) with the settings h.all.v2022.1.Hs.symbols.gmt, 25000 permutations and No_Collapse on the Pearson correlations generated as described from DepMap or TCGA data[75,76]. Gene set enrichment for go term processes was performed using Stringdb “multiple proteins” function on the list of 37 genes significant only in the four *CDS1*-negative cell lines[77].

Lipidomics

Quantitative targeted lipidomics was carried out using a flow-injection assay employing lipid class separation by differential mobility spectroscopy and selective multiple reaction monitoring (MRM) per lipid species (Lipidyzer platform). A detailed description of lipid extraction, software and the quantitative nature of the approach can be found elsewhere[78–80]. Briefly, after the addition of > 60 deuterated internal standards, lipids were extracted using methyl tert-butyl ether. Organic extracts were subsequently dried under a gentle stream of nitrogen and reconstituted in running buffer. Lipids were subsequently analyzed using flow-injection in MRM mode employing a Shimadzu Nexera series HPLC and a Sciex QTrap 5500 mass spectrometer. For further analysis, lipidomic data normalized to cell number was used to calculate the quadruplicate fold changes for plotting and statistical analysis.

Proteomics

Frozen cell pellets were heated for 7 min. at 95^0C in 1x S-Trap Lysis buffer (5% SDS, 50 mM TEAB pH 8.5), after which DNA was sheared by probe sonication. Aliquots comprising 50 µg of protein were reduced with 20 mM DTT (20 min. at 55^0C) and alkylated with 40 mM iodoacetamide (30 min. at room temperature in the dark), after which proteins were digested overnight with trypsin (Sigma-Aldrich; enzyme/substrate ratio 1:10) on S-Trap Micro spin columns according to the manufacturer’s instructions (ProtiFi, NY, USA). Peptides were eluted, vacuum-dried and stored at -80°C until LC-MS/MS analysis. LC-MS/MS was performed by nanoLC-MS/MS on an Orbitrap Exploris 480 mass spectrometer (Thermo Scientific) connected to a Proxeon nLC1200 system. Peptides were directly loaded onto the analytical column (ReproSil-Pur 120 C18-AQ, 2.4µm, 75 µm × 500 mm, packed in-house) and eluted at 250 nL/min in a 90-minutes gradient containing a non-linear increase from 6–30% solvent B (solvent A was 0.1% formic acid/water and solvent B was 0.1% formic acid/80% acetonitrile). The Exploris 480 was run in data-independent acquisition (DIA) mode, with full MS resolution set to 120,000 at m/z 200, MS1 mass range was set from 350–1400, normalized AGC target was 300% and maximum IT was 45ms. DIA was performed on precursors from 400–1000 in 48 windows of 13.5 Da with an overlap of 1 Da. Resolution was set to 30,000 and normalized CE was 27.

RAW files were analyzed with DIA-NN (version 1.8) using standard settings[81]. Fragment spectra were searched against the Swissprot human database (version 2022_02; 20,375 entries) by selecting 'FASTA digest for library-free search'; Trypsin/P was specified as protease specificity allowing a maximum of 1 miscleavage; N-terminal excision (M) and carbamidomethylation (C) were selected as fixed modifications and match between runs was applied. Protein group abundances were extracted from the DIA-NN result files, imported into Perseus (1.6.15.0) and Log2-transformed[82]. For each cell line, values were filtered for presence in at least 4 out of 4 replicates in at least the WT or sg*CDS2* sample group. Missing values were replaced by an imputation-based normal distribution using a width of 0.3 and a downshift of 2.4. Differentially expressed proteins were determined using a two-sided t-test (thresholds: p-value < 0.05 and ^{2}Log abundance ratio [sg*CDS2*/sgControl] < -0.4 ^ > 0.4).

Light microscopy

Live cells stained with BODIPY (2 µM, D3922) were imaged on a regularly maintained Zeiss Axio Observer Z1 microscope at the NKI imaging facility using PhaseContrast- and Fluorescence-equipment. A home-built temperature-controlled live cell chamber and 5% CO_2 incubation system were used. Data was analyzed using a custom ImageJ code. Briefly, for each condition low complexity area on phase contrast was excluded to calculate cell area and BODIPY fluorescence was used to calculate lipid area. Cell lines were imaged 14 days (SK-MEL-2) or 20 days (NCI-H2030) days after transduction.

Electron microscopy

Correlative light electron microscopy (CLEM) was performed as described before[83,84]. Briefly, for CLEM 150–300 nm cryosections of cells were placed onto an EM-grid, stained with Nile red (Sigma, 72485) and Hoechst 33342 (Thermo Fisher, H3570) and imaged with a Wide-field Fluorescence Microscope (Leica DM6, 100x oil objective). After washing and contrasting for EM purposes, the identical grid was imaged using a transmission electron microscope (Talos L120c Thermo Fisher, with Ceta 16M camera).

Statistics and replication

Significance was tested and depicted as indicated. To ensure reproducibility, we addressed experimental variation by including multiple replicates, we addressed biological variation by including multiple cell lines and we employed multiple methods whenever possible.

Methods references

60. Li, W. *et al.* MAGeCK enables robust identification of essential genes from genome-scale CRISPR/Cas9 knockout screens. *Genome Biol.* **15**, 554 (2014).

61. Schindelin, J. *et al.* Fiji: An open-source platform for biological-image analysis. *Nature Methods* **9**, 676–682 (2012).

62. Rahman, M. *et al.* Alternative preprocessing of RNA-Sequencing data in the Cancer Genome Atlas leads to improved analysis results. *Bioinformatics* **31**, 3666–3672 (2015).

63. Eisenberg, E. & Levanon, E. Y. Human housekeeping genes, revisited. *Trends in Genetics* **29**, 569–574 (2013).

64. Li, M., Sun, Q. & Wang, X. Transcriptional landscape of human cancers. *Oncotarget* **8**, 34534–34551 (2017).

65. Zehir, A. *et al.* Mutational landscape of metastatic cancer revealed from prospective clinical sequencing of 10,000 patients. *Nat. Med.* **23**, 703–713 (2017).

66. Apriamashvili, G. *et al.* Ubiquitin ligase STUB1 destabilizes IFNγ-receptor complex to suppress tumor IFNγ signaling. *Nat. Commun.* **13**, 1–16 (2022).

67. Yang, X. *et al.* A public genome-scale lentiviral expression library of human ORFs. *Nat. Methods* **8**, 659–661 (2011).

68. Vredevoogd, D. W. *et al.* Augmenting Immunotherapy Impact by Lowering Tumor TNF Cytotoxicity Threshold. *Cell* **178**, 585-599.e15 (2019).

69. Hanniford, D. *et al.* Epigenetic Silencing of CDR1as Drives IGF2BP3-Mediated Melanoma Invasion and Metastasis. *Cancer Cell* **37**, 55-70.e15 (2020).

70. Young, L., Sung, J. & Masters, J. R. Detection of mycoplasma in cell cultures. *Nat. Protoc.* **5**, 929–934 (2010).

71. Wiernicki, B. *et al.* Excessive phospholipid peroxidation distinguishes ferroptosis from other cell death modes including pyroptosis. *Cell Death Dis.* **11**, 1–11 (2020).

72. Nassour, J. *et al.* Telomere-to-mitochondria signalling by ZBP1 mediates replicative crisis. *Nature* **614**, 767–773 (2023).

73. Sanson, K. R. *et al.* Optimized libraries for CRISPR-Cas9 genetic screens with multiple modalities. *Nat. Commun.* **9**, 5416 (2018).

74. Joung, J. *et al.* Genome-scale CRISPR-Cas9 knockout and transcriptional activation screening. *Nat. Protoc.* **12**, 828–863 (2017).

75. Mootha, V. K. *et al.* PGC-1α-responsive genes involved in oxidative phosphorylation are coordinately downregulated in human diabetes. *Nat. Genet.* **34**, 267–273 (2003).

76. Subramanian, A. *et al.* Gene set enrichment analysis: A knowledge-based approach for interpreting genome-wide expression profiles. *Proc. Natl. Acad. Sci. U. S. A.* **102**, 15545–15550 (2005).

77. Szklarczyk, D. *et al.* STRING v11: Protein-protein association networks with increased coverage, supporting functional discovery in genome-wide experimental datasets. *Nucleic Acids Res.* **47**, D607–D613 (2019).

78. Ghorasaini, M. *et al.* Cross-Laboratory Standardization of Preclinical Lipidomics Using Differential Mobility Spectrometry and Multiple Reaction Monitoring. *Anal. Chem.* **93**, 16369–16378 (2021).

79. Ghorasaini, M. *et al.* Congruence and Complementarity of Differential Mobility Spectrometry and NMR Spectroscopy for Plasma Lipidomics. *Metabolites* **12**, (2022).

80. Su, B. *et al.* A DMS Shotgun Lipidomics Workflow Application to Facilitate High-Throughput, Comprehensive Lipidomics. *J. Am. Soc. Mass Spectrom.* **32**, 2655–2663 (2021).

81. Demichev, V., Messner, C. B., Vernardis, S. I., Lilley, K. S. & Ralser, M. DIA-NN: neural networks and interference correction enable deep proteome coverage in high throughput. *Nat. Methods* **17**, 41–44 (2020).

82. Tyanova, S. *et al.* The Perseus computational platform for comprehensive analysis of (prote)omics data. *Nature Methods* **13**, 731–740 (2016).

83. Grootemaat, A. E. *et al.* Lipid and Nucleocapsid N-Protein Accumulation in COVID-19 Patient Lung and Infected Cells. *Microbiol. Spectr.* **10**, e01271-21 (2022).

84. Bedard, M. *et al.* A terpene nucleoside from M. tuberculosis induces lysosomal lipid storage in foamy macrophages. *J. Clin. Invest.* **133**, e161944 (2023).

Figures

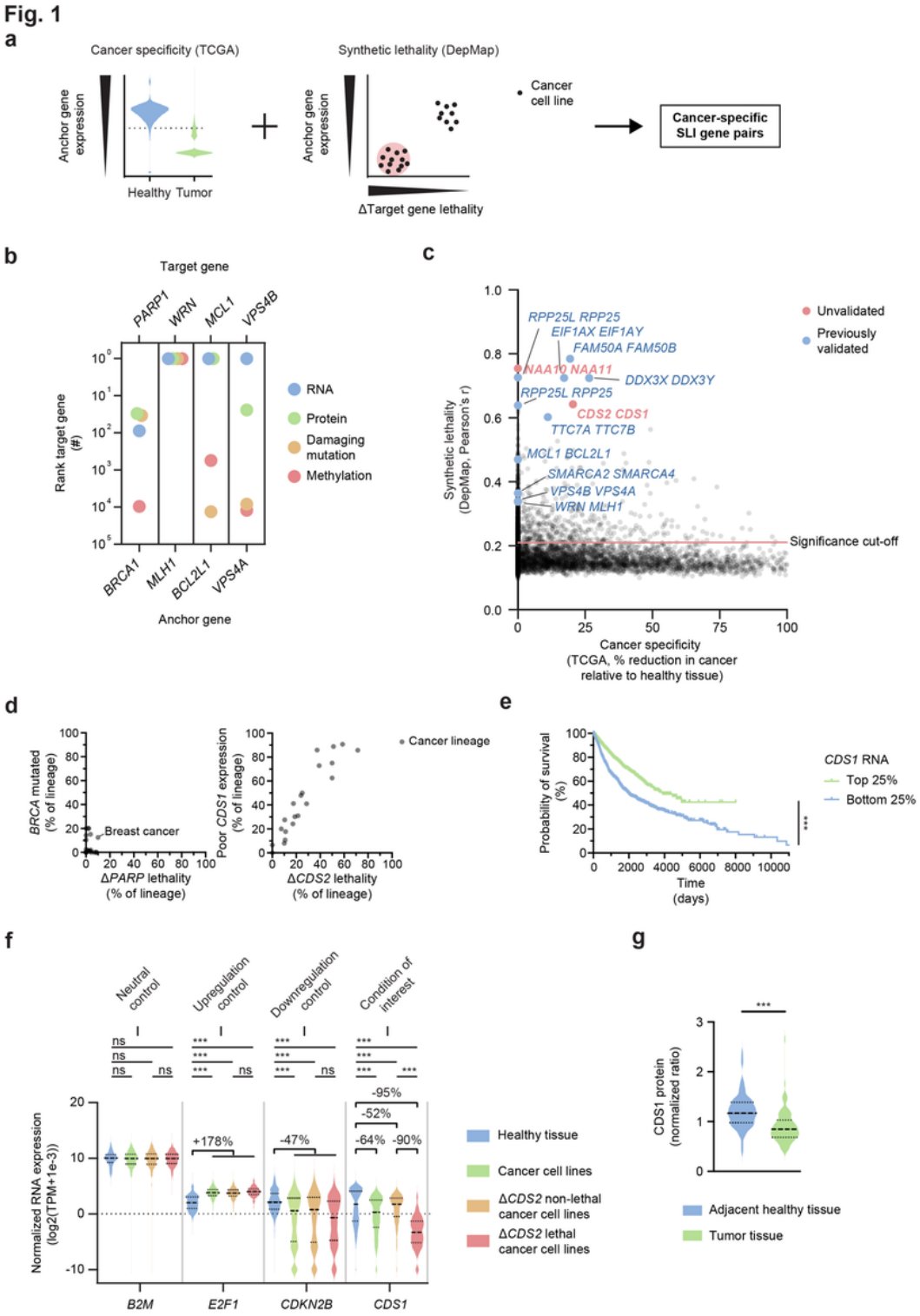

Figure 1

Computational analyses identify *CDS1-CDS2* as a common and cancer-associated SLI

a) Schematic depicting the bioinformatic pipeline for identifying cancer-specific SLIs using TCGA (left) and DepMap (right).

b) The correlation (Pearson's r) between RNA, proteomic, mutation or methylation anchor gene data and gene dependency data in cancer cell lines for previously validated synthetic lethal pairs. The rank of the known target gene partners was plotted for each data type. n (cancer cell lines) = 913 (RNA), 299 (protein), 986 (damaging mutation) and 513 (methylation).

c) Top predicted synthetic lethal pairs, named by their target gene and anchor gene, respectively. Y-axis presents the correlation (Pearson's r) between the expression of the anchor gene and the dependency on the target gene (DepMap). X-axis presents the average reduction in anchor expression in patient tumor samples compared to patient healthy tissue samples (TCGA). Increases in expression are plotted as a 0% reduction. Bonferroni-corrected Pearson-associated p-values were used to determine significance cut-off. n = 913 cancer cell lines and 10.005 patient samples (9264 tumor, 741 healthy).

d) For each cancer lineage the percentage of Δ*CDS2* or Δ*PARP* lethal cancer cell lines (DepMap) was plotted against the percentage of *BRCA1/2*-mutated or low *CDS1*-expressing cancer cell lines. The cut-off for the latter was log2(TPM+1) of 1.5. The cut-off for lethality was CERES<-0.5. A CERES of -1 corresponds to core essential, whereas a CERES of 0 corresponds to non-essential[34]. For each cell line data for the most essential *PARP* gene (out of 13) was included in the analysis. n = 906 cancer cell lines (40 breast).

e) Probability of survival for patients with the highest and lowest quartile of *CDS1* expression of patient tumor samples (TCGA). The hazard ratio for the *CDS1*-low quartile was 1.90 [1.715-2.106] compared to the *CDS1*-high quartile. Log-rank Mantel-Cox test was used. n = 10163 patients.

f) Calibration gene-normalized RNA expression in healthy tissue samples (GTEx), cancer cell lines (DepMap), Δ*CDS2* lethal cancer cell lines (DepMap, CERES<-0.5) and Δ*CDS2* non-lethal cancer cell lines (DepMap, CERES>-0.5) are presented in violin plots for the genes *B2M*, *E2F1*, *CDKN2B* and *CDS1*. The three dotted lines in each violin represent the quartile cut-offs. For significant differences the percentual change in average TPM was indicated. For controls one overall average was indicated. Kruskal-Wallis test followed up by Dunn's test was used. n = 17382 healthy tissue samples and 913 cancer cell lines (657 Δ*CDS2* non-lethal and 256 Δ*CDS2* lethal).

g) Calibration gene-normalized CDS1 protein levels in matched healthy lung and lung tumor samples[47]. The three dotted lines in each violin represent the quartile cut-offs. Mann-Whitney test was used. n = 110 tumor samples and 102 adjacent healthy lung samples.

P-values were indicated by * (<0.05), ** (<0.01) and *** (<0.001).

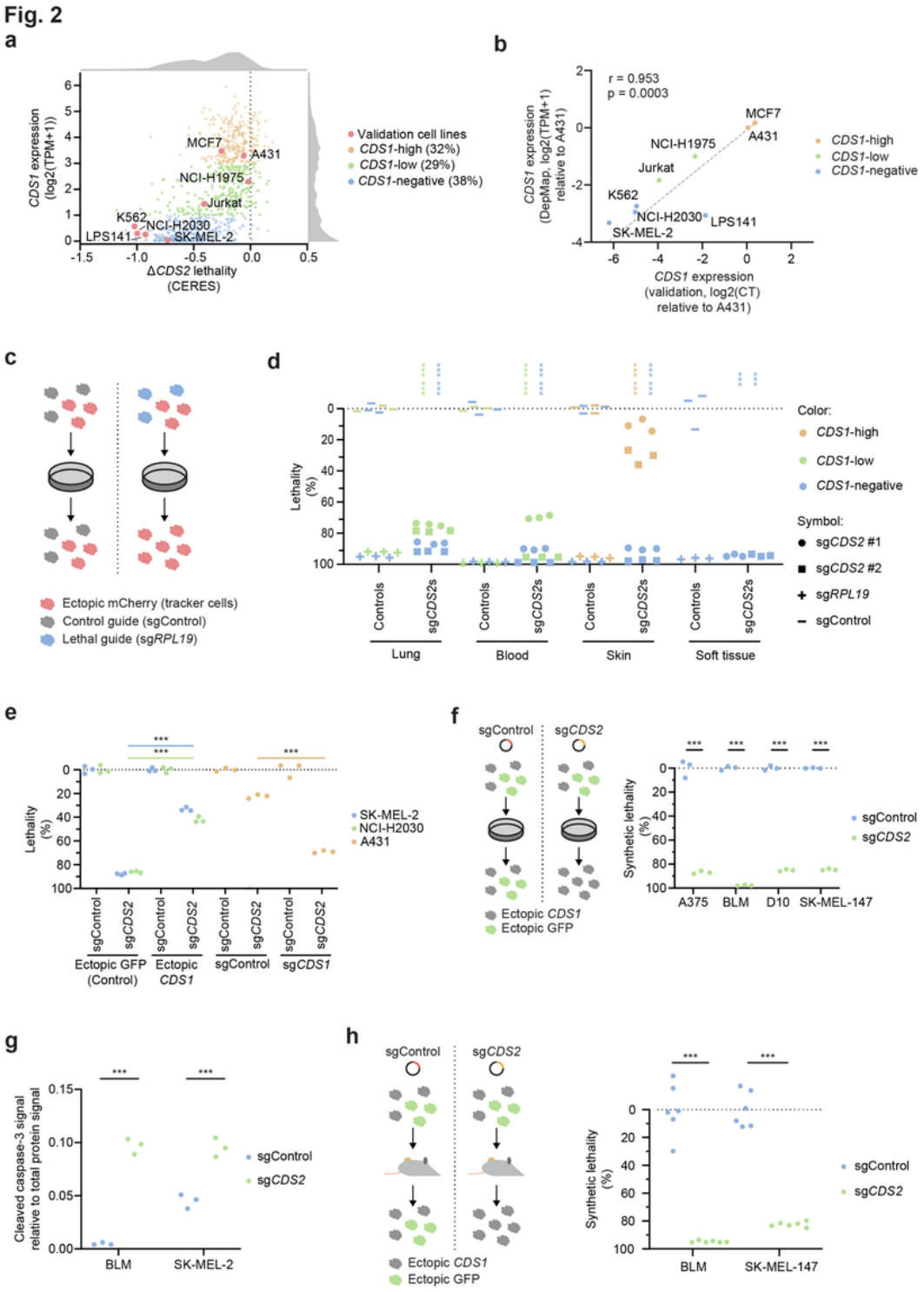

Figure 2

CDS1 and *CDS2* constitute a synthetic lethal gene pair across cancer types *in vitro* and in melanoma *in vivo*

a) Plot depicting synthetic lethality upon CRISPR perturbation of *CDS2* (Δ*CDS2* lethality) and *CDS1* RNA expression for cancer cell lines (DepMap). Cancer cell lines were categorized by *CDS1* RNA levels and cell

lines used for validation are marked. Histograms depicting the distribution were added for both axes. n = 913 cancer cell lines.

b) Plot depicting *CDS1* RNA expression as measured by RNA sequencing (DepMap) or qPCRanalysis. The correlation (Pearson's r) and the associated p-value (p) were added. Average of two independent experiments with each n = 4 replicates for 8 cancer cell lines.

c) Diagram depicting the method for quantifying lethality upon CRISPR perturbation using fluorescent tracker cells. The mCherry-positive percentage was quantified by flow cytometry.

d) Graph depicting cumulative lethality 14d after CRISPR perturbation of *CDS2*using tracker cells (panel c). *CDS2* sgRNAs, positive control sgRNA (*RPL19*) and negative control sgRNA (sgControl) were included. Two-way ANOVA followed up by Dunnett's test was used. n = 3 replicates for 7 cancer cell lines with 2 *CDS2* sgRNAs. Independent experiment repeat in panel e (3 cancer cell lines) and Fig. 3b (4 cancer cell lines); the latter also includes an additional *CDS1*-high cancer cell line.

e) For two *CDS1*-negative cell lines (NCI-H2030 and SK-MEL-2) *CDS1* or GFP (control) was ectopically expressed and 14d Δ*CDS2* lethality was determined using tracker cells (panel c). For one *CDS1*-high cell line *CDS1*(sg*CDS1*, versus sgControl) was perturbed by CRISPR and 8d Δ*CDS2* lethality was determined using tracker cells (panel c). Two-way ANOVA followed up by Tukey's test was used. n = 3 replicates for 3 cancer cell lines, A431 and NCI-H2030/SK-MEL-2 are separate experiments.

f) Left: diagram depicting method for quantifying synthetic lethality using ectopic *CDS1* or GFP expression. The GFP-positive percentage was quantified by flow cytometry. Right: graph depicting quantification of synthetic lethality in melanoma. Two-way ANOVA followed up by Sidak's test was used. n = 3 replicates for 4 cancer cell lines.

g) Graph depicting snapshot of the total protein normalized level of cleaved caspase-3 in Δ*CDS2* or control samples of BLM and SK-MEL-2 cell lines, as determined by quantitative western blotting (Abby). Two-way ANOVA followed up by Sidak's test was used. n = 3 replicates for 2 cancer cell lines.

h) Left: diagram depicting the *in vivo* variant of the method for quantifying synthetic lethality. Right: graph depicting quantification of the *in vivo* synthetic lethality in two melanoma cell line models. Two-way ANOVA followed up by Sidak's test was used. n = 6 NOD-Scid IL2Rgnull mice per group each for 2 cancer cell lines.

P-values were indicated by * (<0.05), ** (<0.01) and *** (<0.001).

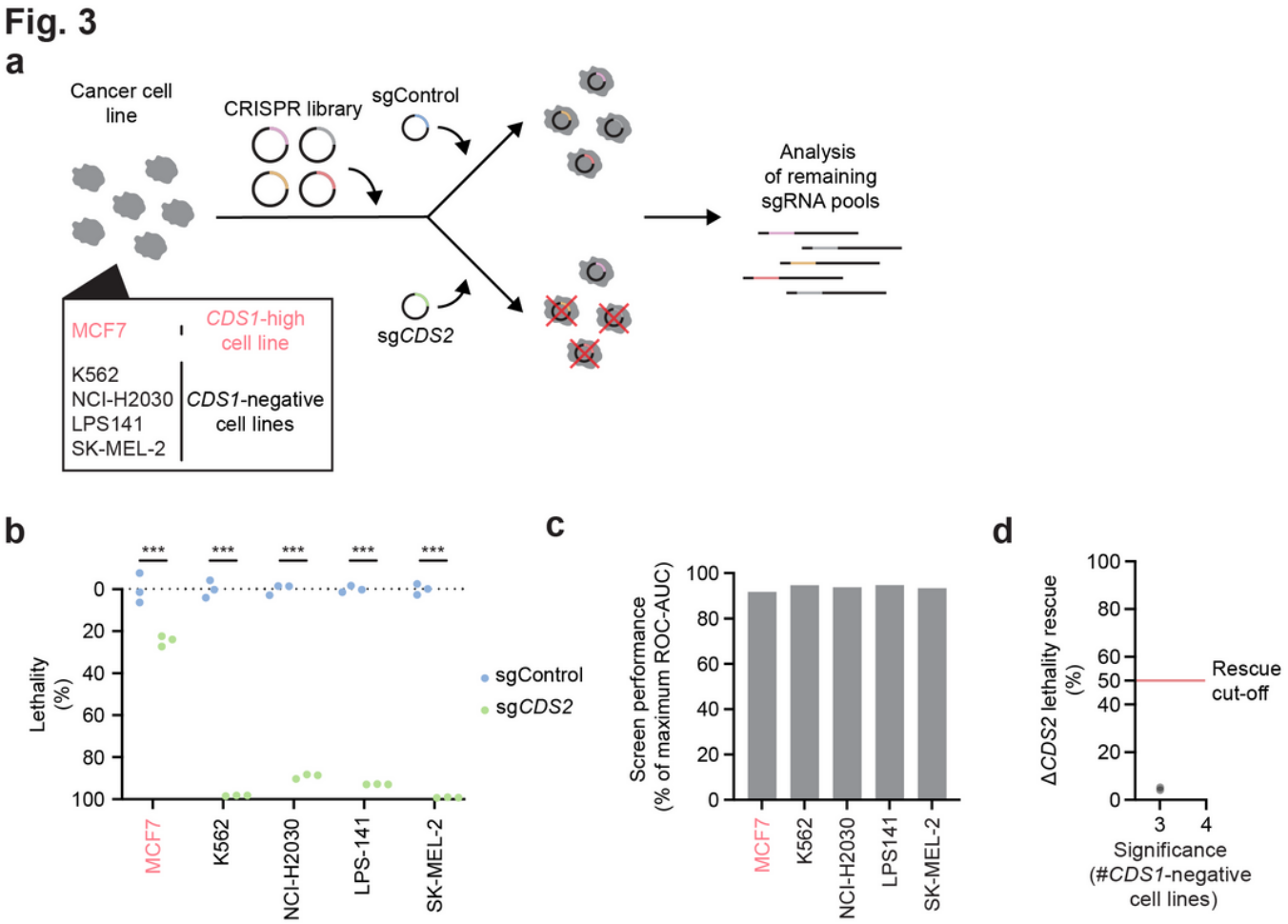

Figure 3

No common escape mechanism for Δ*CDS2* lethality

a) Diagram depicting the method used to screen for Δ*CDS2* lethality escape mechanisms. One *CDS1*-high cancer cell line and four *CDS1*-negative cancer cell lines were screened.

b) The lethality of the screen cells between day 15 and day 25. Lethality was quantified using fluorescent tracker cells as depicted in Fig. 2c. Two-way ANOVA followed up by Sidak's test was used. n = 3 replicates for 5 cancer cell lines.

c) As a quality control, each control arm was compared with the original library to detect essential genes (true positives) over non-essential genes (true negatives). The resulting area under the receiver operator curve (ROC-AUC) values for each screen are presented. A ROC-AUC above 90% of maximum is considered outstanding for CRISPR screens[73]. n = 1 for 5 cancer cell lines at 200x coverage with 4 sgRNA per gene and 1000 sgControls in the CRISPR library.

d) Graph depicting the screen hits identified in 3/4 or all 4 *CDS1*-negative cancer cell lines. Effect size was calculated using the average Δ*CDS2* lethality in the lethality assays with screen cells (panel b) and the fold-change enrichment of the second-best guides for each gene. Benjamini-Hochberg corrected p-values from MAGeCK resulted in the indicated significance. n = 1 for 4 cancer cell lines at 200x coverage with 4 sgRNA per gene and 1000 sgControls in the CRISPR library.

P-values were indicated by * (<0.05), ** (<0.01) and *** (<0.001).

Fig. 4

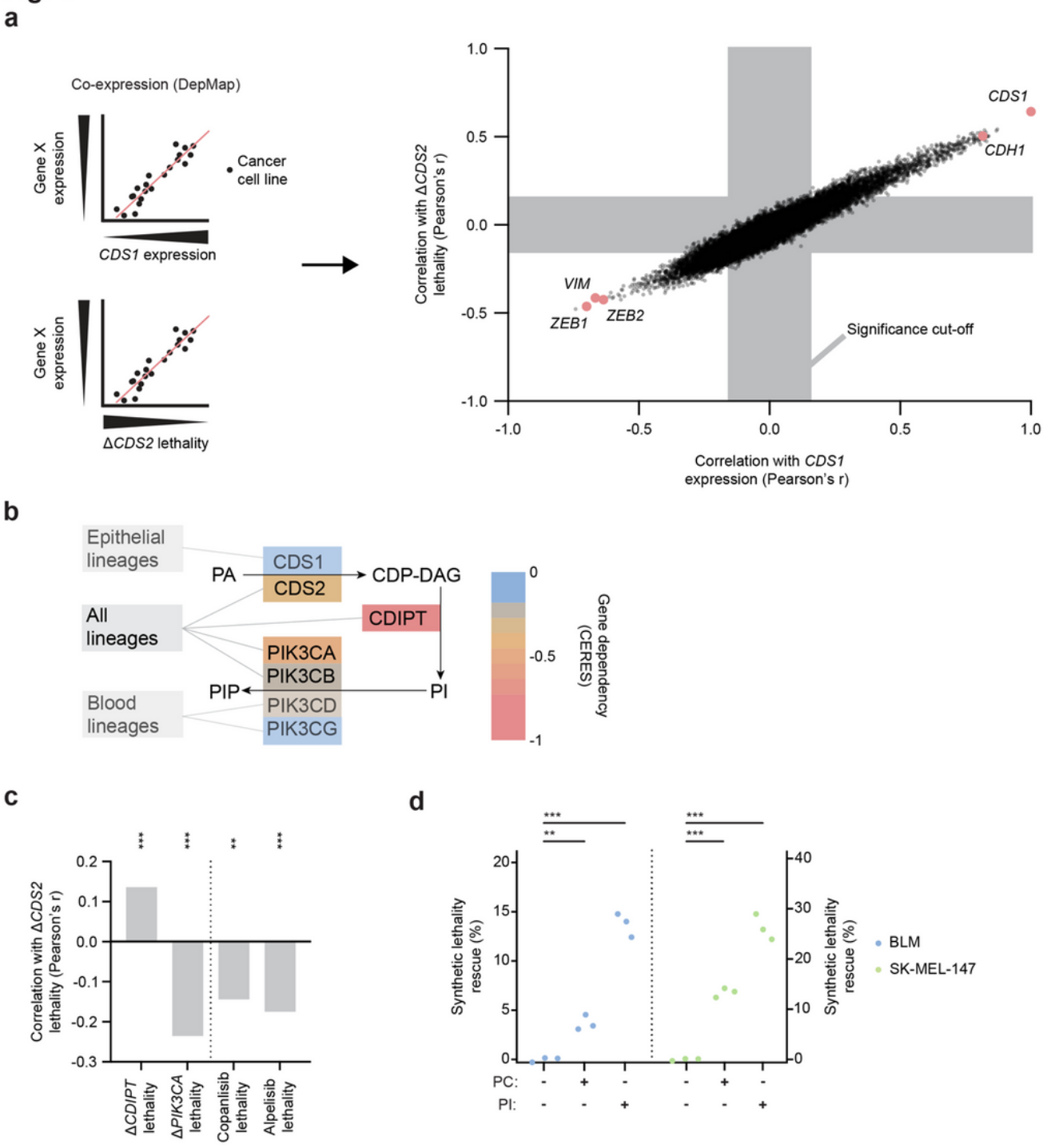

Figure 4

Mesenchymal cancers depend on *CDS2* for PI synthesis

a) Left: method for phenotyping Δ*CDS2* lethal/*CDS1*-low cancer cell lines and Δ*CDS2* non-lethal/*CDS1*-high cancer cell lines (DepMap) (illustrative). Right: genome-wide calculated Pearson correlations. Five genes enriched on either side are marked. Bonferroni corrected Pearson associated p-values were used to determine significance cut-off. n = 913 cancer cell lines.

b) Diagram depicting the core CDS1/2 pathway. The lethality upon perturbation (color) and lineage specific expression patterns (grey boxes on the left) of each enzyme in the pathway are indicated (DepMap). For abbreviations, see bottom of figuredescription. Gene dependency is represented by CERES. n = 913 cancer cell lines.

c) Correlation between Δ*CDS2* lethality and Δ*CDIPT* lethality, Δ*PIK3CA*lethality, PIK3CA inhibitor lethality (Alpelisib) or the pan-PI3K inhibitor lethality (Copanlisib) in solid cancer cell lines (DepMap). The Bonferroni corrected Pearson correlation associated p-values were used. n (cancer cell lines) = 865 (*CDIPT* and *PIK3CA*), 428 (Copanlisib) and 441 (Alpelisib).

d) Rescue of synthetic lethality upon supplementation with phosphatidylinositol (PI) or phosphatidylcholine (PC, control). The method to quantify synthetic lethality was introduced in Fig. 2f. PI and PC were complexed with lipid free bovine serum albumin. Two-way ANOVA followed up by Dunnett's test was used. n = 3 replicates for 2 cancer cell lines.

P-values were indicated by * (<0.05), ** (<0.01) and *** (<0.001).

PA = phosphatidic acid, CDS = cytidine diphosphate diacylglycerol synthase, CDP-DAG = cytidine diphosphate diacylglycerol, CDIPT = cytidine diphosphate diacylglycerol synthase inositol-3-phosphatidyltransferase, PI = phosphatidylinositol, PIK3C = phosphatidylinositol-4,5-bisphosphate 3-kinase, PIP = phosphatidylinositol phosphate

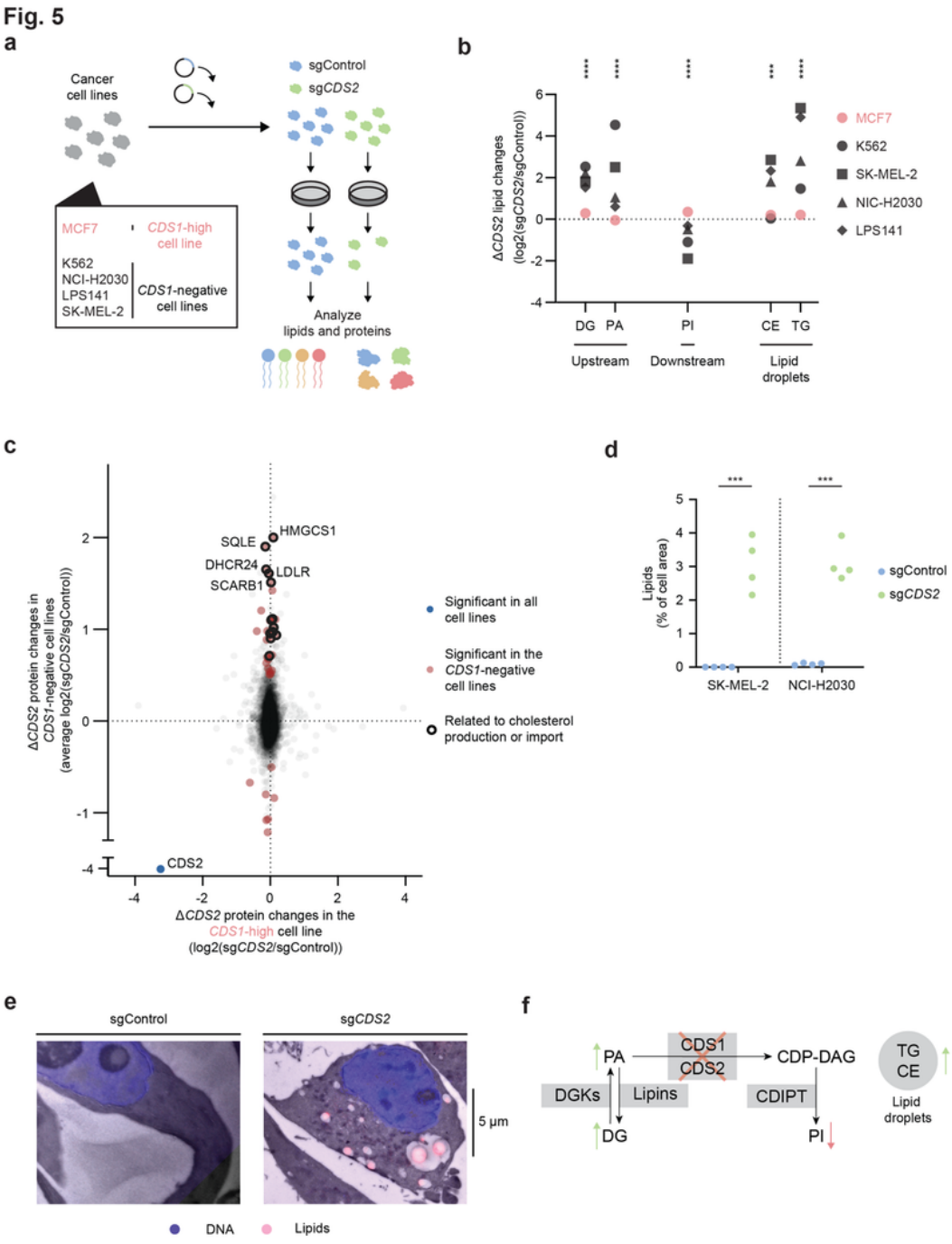

Figure 5

Expression of either *CDS1* or *CDS2* is required for lipid homeostasis

a) Diagram depicting the samples generated for quantifying lipids and proteins. One *CDS1*-high cancer cell line and four *CDS1*-negative cancer cell lines were analyzed.

b) Five Δ*CDS2* lipid class changes are presented (full results in Extended Data Fig. 5a). The stars indicate the number of *CDS1*-negative cell lines with at least two-star significant lipid alterations compared to the *CDS1*-high cell line. Two-way ANOVA followed up by Sidak's test was used. n = 4 replicates for 5 cancer cell lines.

c) Average Δ*CDS2* protein changes for the four *CDS1*-negative cancer cell lines (y-axis) were plotted against the Δ*CDS2* protein changes in the *CDS1*-high cancer cell line (x-axis). Significance was determined by students T test. n = 4 replicates for 5 cancer cell lines.

d) Cell areas staining positive for the lipid compartment dye BODIPY in live cell imaging. Two-way ANOVA followed up by Sidak's test was used. n = 4 replicates for 2 cancer cell lines.

e) Representative combined light and transmission electron microscopy image of a sgControl and a sg*CDS2* SK-MEL-2 cell stained for lipids (Nile Red) and DNA (Hoechst). n = 1 for 1 cancer cell line, an independent experiment was performed for quantification (panel d).

f) Cartoon depicting lipid compartments and the CDS2 pathway. The Δ*CDS2* lipid class changes in the four *CDS1*-negative cell lines are marked by arrows. Abbreviations below.

(b) Significance was indicated by one * for each cell line with p-value<0.01 (d) P-values were indicated by * (<0.05), ** (<0.01) and *** (<0.001).

DG = diacylglycerol, DGKs = diacylglycerol kinases, PA = phosphatidic acid, CDS = cytidine diphosphate diacylglycerol synthase, CDP-DAG = cytidine diphosphate diacylglycerol, PA = phosphatidic acid, CDIPT = cytidine diphosphate diacylglycerol synthase inositol-3-phosphatidyltransferase, PI = phosphatidylinositol, TG = triglycerides, CE = cholesterol esters

Supplementary Files

This is a list of supplementary files associated with this preprint. Click to download.

- SupplementaryTable1.xlsx
- SupplementaryTable2.xlsx
- SupplementaryTable3.xlsx
- SupplementaryTable4.xlsx
- SupplementaryTable5.xlsx
- SupplementaryTable6.xlsx
- ExtendedDataFigure.docx